2023-01-1686 Published 31 Oct 2023

A Novel 1-ϕ Cuk Based On-Board EV Charger with Minimal Power Components

Phani Kumar Chamarthi and Christopher Edrington Clemson University

Ali Arsalan CU-ICAR Clemson Univ Int'l Center For Au

Laxman Timilsina Clemson Univ

Behnaz Papari and Gokhan Ozkan Clemson University

Ali Moghassemi Clemson Univ

Citation: Chamarthi, P.K., Edrington, C., Arsalan, A., Timilsina, L. et al., "A Novel 1-ϕ Cuk Based On-Board EV Charger with Minimal Power Components," SAE Technical Paper 2023-01-1686, 2023, doi:10.4271/2023-01-1686.

Received: 15 Jun 2023 Revised: 29 Aug 2023 Accepted: 06 Sep 2023

Abstract

This paper proposes a novel 1-ϕ, Cuk based on-board electric vehicle (EV) charger with least power components. The proposed EV charger has a special feature to achieve power factor correction (PFC) at AC grid without requirement of the grid voltage and current sensors which cuts the cost and increases the power density of the EV charger along with robustness to noise. The automatic PFC at AC grid is accomplished by operating the output DC inductor in discontinuous conduction mode (DCM). The proposed EV charger necessitates a minimal number of power components for positive and negative half cycles of AC grid which improves the overall efficiency of the system. This is possible due to the combination of inverting and non-inverting Cuk converters are used for each half cycle of the AC grid. Further, the presence of output inductor in the EV charger reduces the ripples in the output current which is not common with all the existing chargers in the literature. In addition, the control of charger is simple, and easy to implement with only battery current sensor based current control. The proposed charger configuration has lower voltage stress across the power switches and diodes in comparison with the existing charger configurations. The theoretical concept is validated through experimental studies which prove the superior execution of PFC control of the 2kW EV charger. The various performance factors such as power factor at AC grid is 0.996 and total harmonic distortion (THD) in the AC grid current is 2.8% which are within the limits of standard IEC 61000-3-2.

Introduction

Nowadays research on electric vehicles (EVs) has been speeding up due to increasing awareness on environmental conditions [1, 2, 3]. These EVs supported by batteries alleviate to build a noiseless and lesser polluted environment while reducing the operational cost [3, 4, 5]. Several industries and government organizations have been showing interest in these technologies which are funded by numerous government advancement programs [6, 7, 8, 9]. One of the survey reports in 2019 says that approximately 6 million EVs are on the street and by 2050, the EVs on the street will be 1 billion [10, 11, 12]. Usually, the voltage ratings of batteries for EVs varies from 400V to 600V. Hence a charger is needed to charge the EV battery. Currently, the EV chargers are categorized in to two types [13, 14, 15, 16].

- On-board charger
- Off-board charger

The main role of EV charger is to provide a commanded DC power at the output by converting the utility AC power [10]. In addition, to maintain the harmonic constraints a power factor correction converter (PFCC) is employed at the front end of EV charger [19]. Usually, a regular EV charger contains an input AC filter, an AC-DC rectifier as PFCC and DC-DC converter which are connected in a cascaded manner as shown in Fig. 1 [17].

FIGURE 1 Conventional Grid to Vehicle (G2V) on/off-board charger [17].

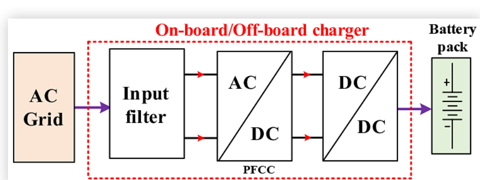

Several researchers have proposed EV charger configurations which are two-stage systems (i.e., PFCC followed by DC-DC converter) [2, 6, 17, 18, 19]. The two-stage EV charger configurations have an advantage of easiness in implementation, but these configurations have several major drawbacks such as a greater number of components, higher power losses and lower efficiency. The higher the number of components in the system, the increases the system size as well as cost. To overcome above mentioned disadvantages, single-stage charger configurations have been introduced by some researchers [20, 21, 22, 23, 24, 25, 26, 27, 28, 29, 30]. The single-stage configurations in [20] and [21] are obtained by combining AC-DC diode rectifier and DC-DC converters. However, the diode rectifier at the input is lossy and necessitates an alternate solution (i.e., EV charger without diode rectifier) [22, 23, 24, 25, 26, 27, 28, 29, 30]. Although the single stage configurations in [17, 22, 23, 24, 25, 26, 27, 28, 29, 30] doesn't incorporate diode rectifier but the number of power components are same as traditional configurations.

For instance, the introduced single stage EV charger topologies in [20] are shown in Fig. 2(a), Fig. 2(b), and Fig. 2(c) respectively. The EV charger topology in Fig. 2(a) has advantages of lower input current ripple and simple operation. However, it has drawbacks of circulating currents through two auxiliary capacitors in both half cycles of grid voltage which incorporates additional losses in the system. Whereas the EV charger topology in Fig. 2(b) incorporates additional inductor at the output which provides improved thermal management to the system. Conversely, this adds a greater number of power components to the system which also includes two extra capacitors in the output. Another drawback of this topology is that the load is located between the two output capacitors which makes the EV charger output terminals float. The EV charger topology in Fig. 2(c) has lower current stress across power components; however, the body diode of stationary switch continuously conducts in every half cycle of grid voltage which incurs additional losses in the system. For example, in the positive half cycle of the grid, the body diode of stationary switch S_2 conducts via output inductor L_2 due to part of return current in the circuit which encounters extra power losses. Fig. 2(d) and Fig. 2(e) shows two different EV charger configurations (i.e., in [23] and [24]) which have almost same number of power components as conventional Cuk PFCC (i.e., Fig. 2(d) has 9 components whereas Fig. 2(e) has 10 components). Furthermore, these EV charger configurations also have the same stress across power devices like conventional Cuk PFCC.

However, these EV charger configurations experience high input and output current ripples due to problem of inductor coupling which eventually impacts the life of the battery. The EV charger configuration shown in Fig. 2(f) is simple in implementation and easy to control [21]. Further, the current stress of the components is same as traditional Cuk PFCC in DCM however, this topology experiences higher voltage stress across power switches and higher THD in input current. In addition, this charger configuration necessities extra input filter. Thus, taking a cue from the above-mentioned configurations, this paper proposes a novel Cuk based EV charger configuration with minimal power components and easy control strategy in comparison to existing EV charger configurations.

The distinguishing features of the proposed EV charger configuration are given as follows:

- It requires optimized/reduced number of components with lower voltage stress across the semiconductor devices.
- The output inductor operates in DCM to achieve automatic PFC at AC grid.
- The natural PFC at AC grid eliminates the necessity of AC voltage and current sensors which enhances the power density, cuts the cost of the system.
- The PFC is achieved with only one output current control which requires only one current sensor. Therefore, the closed loop control of converter is easy and simple for implementation which increases the reliability of system.
- The voltage stress across power semiconductor devices is lower hence switching losses are reduced and a lower

FIGURE 2 Some of the existing on-board EV chargers in the literature; (a)-(c) [20], (d) [23], (e) [24], (f) [21]

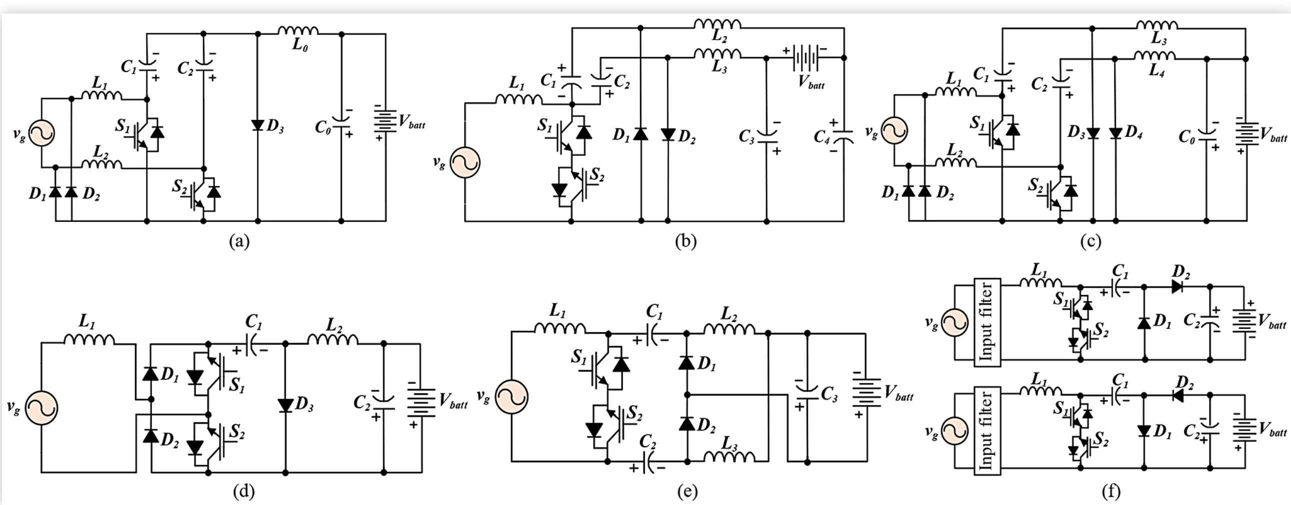

number of devices are in conduction path which reduces the conduction losses. Thus, overall efficiency of the system is enhanced.

The paper is organized as follows: Introduction section discusses the various EV charger configurations in the literature. Next section presents the proposed EV charger configuration and its various modes of operation along with the design of power components. 3rd section discusses the modulation and control strategies of proposed EV charger along with the comparison of proposed converter with the several existing charger configurations. The experimental results to prove the validity of the proposed EV charger configuration are shown to check the accurateness of the closed loop control which are presented in the 4th section. The last section discusses the important conclusions drawn from the proposed work.

Configuration and Operation of Proposed Cuk EV Charger

The proposed charger configuration is derived from basic Cuk converter configurations (i.e., Inverting, and non-inverting converters) as shown in Fig. 3. The converters shown in Fig. 3 are fused into one system in such a way that they can operate during positive and negative half cycles of the AC grid. The output voltage of the system can be higher or lower than input voltage due to natural buck and boost capabilities of Cuk converter configuration.

Fig. 4 shows the proposed Cuk based EV charger. It consists of two inductors (L_g and L_0), three switches (S_1 to S_3), two power diodes (D_1 and D_2) and two capacitors (C_A and C_0). It can be observed that the total power components required for the proposed EV charger is nine whereas existing charger configurations utilize more than nine power components. The series connected switches (S_1 and S_2) in the proposed system provides blocking capability in both positive and negative

FIGURE 3 Conventional Cuk converters; (a) inverting, (b) non-inverting.

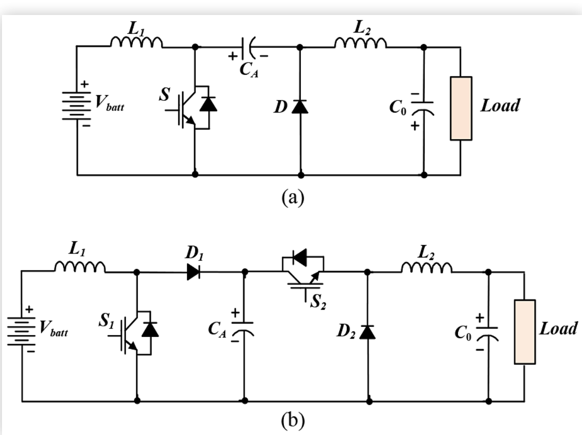

FIGURE 4 Proposed Cuk based on board EV charger.

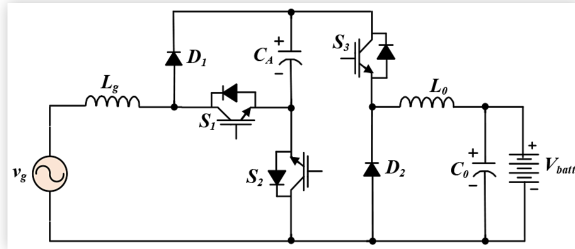

cycles of the AC grid and these two switches are switched ON and OFF during the operation of charge as given in Table 1. As shown in Fig. 4 the proposed charger consists of output inductor L_0 which smoothens the ripples in the output current so that the lesser value of the output capacitor can be realized. Other than this, charger can eliminate the requirements of the dead band between the switches due to the presence of output inductor which evades the shoot through issues.

The various modes (total six) of operation of the charger are shown in Fig. 5(a), Fig. 5(b), Fig. 5(c), Fig. 5(d), Fig. 5(e), and Fig. 5(f) for the case of discontinuous conduction (i.e., $i_{L0}=0$). Fig. 5(a), Fig. 5(b), and Fig. 5(c) correspond to the modes of operation in the positive half cycle (i.e., Mode-I to Mode-III) and Fig. 5(d), Fig. 5(e), and Fig. 5(f) correspond to the modes of operation in the negative half cycle of grid voltage (i.e., Mode-IV to Mode-VI). The switching states corresponding to the modes-I to VI are given in Table 1.

In Mode-I, the switches S_1 and S_3 are turned ON. During this mode, the inductor L_g stores energy from the input source. The auxiliary capacitor C_A transfers its energy to the battery through the switch S_3, output inductor L_0 as shown in Fig. 5(a). During this mode the output inductor L_0 stores energy from capacitor C_A. In Mode-II, the power switches S_1 and S_3 are turned OFF. During this mode, the stored energy in the L_g is transferred to the auxiliary capacitor C_A and the energy stored in the L_0 (i.e., $i_{L0}>0$) free wheels through the power diode D_2 and output capacitor C_0 via battery as shown in Fig. 5(b). During the discontinuous mode (DCM) of operation, the current through $i_{L0}=0$ and the energy stored in the inductor L_g is continue transferring energy to C_A as shown in Fig. 5(c).

Similarly, in the negative half cycle (i.e., in Mode-IV) L_g stores energy and auxiliary capacitor C_A transfers its energy to the battery by using power switches S_1, S_2 and S_3 as shown in Fig. 5(d). The stored energy in L_g gets transferred to auxiliary capacitor C_A in Mode-V by using power switches S_1, S_3 and diode D_2 as shown in Fig. 5(e). During this mode, the

TABLE 1 Switches ON/OFF condition w.r.t modes of operation

	Switches States (1=on, 0=off)					
	S_1	S_2	S_3	D_1	D_2	Mode
+ve half cycle	1	0	1	0	0	I
	0	0	0	1	1	II
	0	0	0	1	0	III
-ve half cycle	0	1	1	0	0	IV
	0	0	0	0	1	V
	0	0	0	0	1	VI

FIGURE 5 Working modes of Proposed Cuk based on board EV charger during DCM operation.

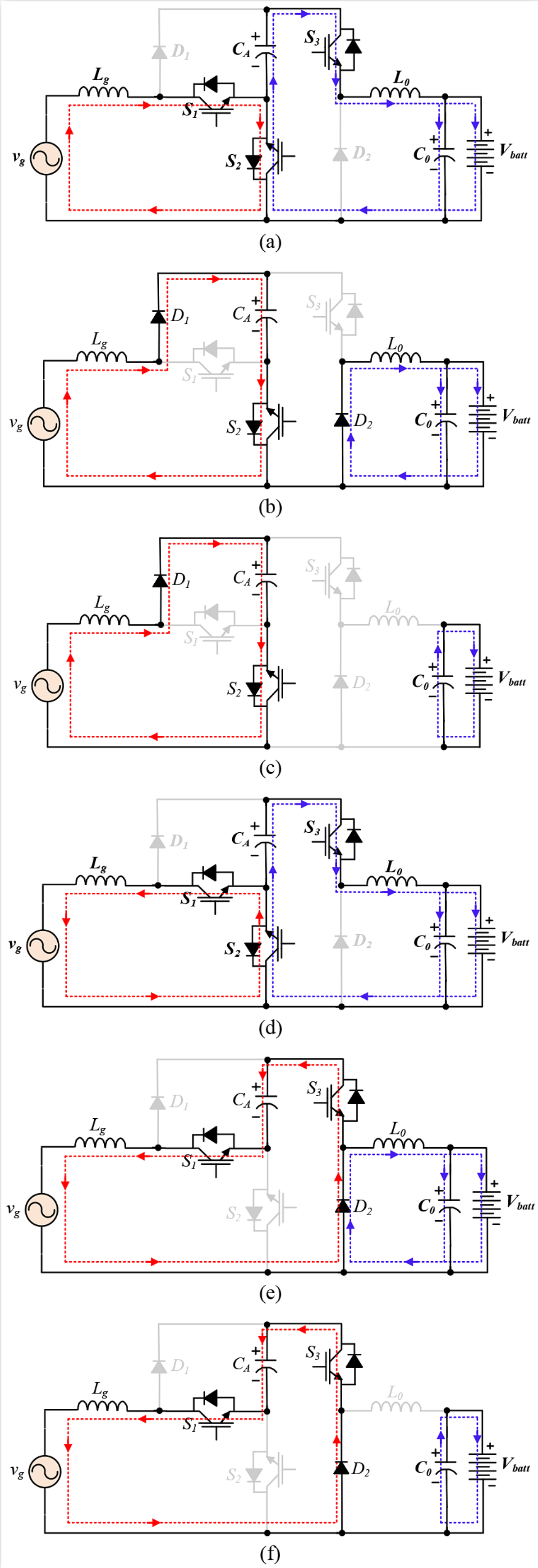

energy stored in "L_0" free wheels through diode D2 and C_0 via battery. During the DCM operation, the current through i_{L0}=0 and the energy stored in the inductor L_g free wheels through the switches S_1, S_3 and diode D_2 as shown in Fig. 5(f).

In case of DCM operation, $t_{on}+t_{off} < T_S$ where t_{on}, t_{off} are ON and OFF durations of switch S_1. Here $t_{on}= D\times T_S = m_a\times sin(\omega t)\times T_S$ and t_{off} can be calculated by using voltage across inductor 'L_g'.

$$\left.\begin{aligned} v_g \times t_{on} &= \left(V_{C_A} - v_g\right)\times t_{off} \\ t_{off} &= \frac{v_g \times t_{on}}{\left(V_{C_A} - v_g\right)} \end{aligned}\right\} \tag{1}$$

Design of the EV Charger Components

This section discusses the design aspects of the various power components in the EV charger.

Design of Output Inductor (L_0) The design specifications considered for the output inductor (L_0) are 2kW and switching frequency of 20kHz. Here, L_0 is considered to be operating in DCM and it stores energy from C_A when S_1 is switched ON. Hence, the voltage across L_0 can be expressed as below.

$$\left.\begin{aligned} V_{C_A} - v_{batt} &= L_0\left(\frac{di_{L_0}}{dt}\right) \\ L_0 &= \left(V_{C_A} - v_{batt}\right)\left(\Delta T / \Delta i_{L_0}\right) = \left(V_{C_A} - v_{batt}\right)\left(m_r T_S / I_{L_{0max}}\right) \end{aligned}\right\} \tag{2}$$

Where V_{CA} is the voltage across auxiliary capacitor, v_{batt} is the voltage across battery and I_{L0max} is the maximum current flowing through inductor.

Design of Grid Inductor (L_g) The grid inductor (L_g) can be designed by using the following expression.

$$L_g = \frac{1}{C_g\left(2\pi f_c\right)^2} \tag{3}$$

Here C_g is the capacitor connected across AC grid and f_c is the cutoff frequency which is 1/10th of the f_s.

Design of Auxiliary Capacitor (C_A) The expression to calculate the value of auxiliary capacitor (C_A) is given below.

$$C_A = \frac{1}{w_r^2\left(L_g + L_0\right)} \tag{4}$$

Here, w_r is the resonance frequency and the value of w_r is selected such that its value is al6ways lesser than w_s (i.e. $2\pi f_s$) and greater than w_g (i.e. $2\pi f_g$).

Design of Output Capacitor (C_0) The output capacitor (C_0) is charged and discharged depends on the modes of operation of the EV charger. The rate at which C0 is charged/discharged can be assessed with the expression given below.

$$\frac{\Delta Q_{C_0}}{\Delta T_s} = C_0\left(\frac{\Delta v_{C_0}}{\Delta T_s}\right) = i_0 \tag{5}$$

Here, ΔQ_{C0}, Δv_{C0} and ΔT_s are change in charge, voltage ripple and charging/discharging times of the C_0. 'i_0' is the output current which is flowing through C_0. Hence, it can be understood that the value of C_0 is determined with the help of output power (P_0) and output capacitor voltage ripple (Δv_{C0}) as given below.

$$C_0 \geq \frac{P_0}{v_{C_0} \Delta v_{C_0} f_S} \quad (6)$$

Here, the ripple Δv_{C0} is considered to be 5% and f_S is the inverter's switching frequency.

Design of Semiconductor Devices (S_1~S_3, D_1 and D_2)

The mean current flowing through the semiconductor devices in one switching cycle can be detemined by using expressions given below.

$$i_{S_1} = i_{S_2} = i_{S_3} = i_{D_1} = i_{D_2} = \sqrt{2} \times i_g \quad (7)$$

Here, i_{S1}, i_{S2}, i_{S3}, i_{D1} and i_{D2} represntes the mean/average current flowing thorugh power devices S_1, S_2, S_3, D_1 and D_2 respectively. 'i_g' represents the grid current RMS value. In a similar manner, the mean/avergae voltages across semiconductor devices in one switching cycle can be expressed as (8).

$$\begin{aligned} v_{S_1} &= v_{S_1} = v_{D_1} = v_{C_A} = \frac{1}{1-m_r}\left(\sqrt{2} \times v_g\right) \\ v_{D_2} &= v_{C_0} = \frac{m_r}{1-m_r}\left(\sqrt{2} \times v_g\right) \\ v_{S_3} &= v_{C_A} - v_{C_0} = \sqrt{2} \times v_g \end{aligned} \quad (8)$$

Control and Modulation Methods of EV Charger

This section presents the modulation and control techniques adopted for the proposed EV charger. Fig. 6(a) and Fig. 6(b) shows the modulation technique in the positive and negative cycles of the AC grid respectively. Fig. 6(c) shows the simple current control strategy used to charge the battery at 2kW.

The modulation strategy shown in Fig. 6(a) and Fig. 6(b) shows that the modulating wave (v_m) is compared to the triangular wave (v_{tr}) to generate gate pulses to the switches S_1, S_2 and S_3 (i.e., g_{S1}, g_{S2} and g_{S3}).

The modulation ratio of the proposed charger configuration can be expressed as given below.

$$\frac{v_0}{\hat{v}_g} = \frac{m_r}{1-m_r} \quad (9)$$

Here, v_0, v_g and m_r are the average output voltage, peak grid voltage and modulation ration of the charger respectively. The proposed charger is compared with the other charger configurations [20]-[29] as given in Table 2. Several existing charger configurations consist of a greater number of inductors and capacitors which increases the size and weight of the charger and reduces reliability. Further, the proposed charger configuration requires only one sensor for the closed loop control (show in Fig. 6(c)). In addition, the increase in the component count increases the cost of the system and occupies more space on the EV. The complete comparison of the proposed charger configuration with other existing charger configurations is given in Table 2.

FIGURE 6 Generation of gate pulses and closed loop control strategy.

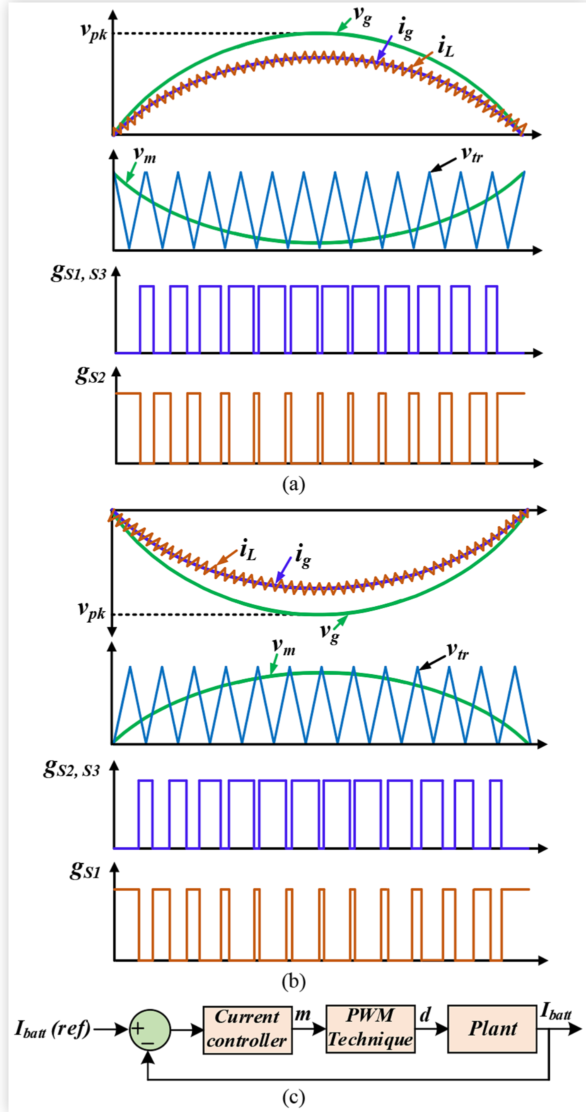

Experimental Validation

To verify the design and prove the validity of proposed charger configuration (Fig. 4) a laboratory prototype has been built for a power rating of 2kW. The parameters used for experimental study are given in Table 3. The design of the grid inductance (Lg) is performed by considering the ripple in current (i.e., 5%) and least possible grid voltage condition.

The experimental results of the proposed charger configuration for full load are shown in Fig. 7. It can be observed that the proposed EV charger can achieve the PFC for power ratings of 1kW and 2kW respectively (shown in Fig. 7(a) and Fig. 7(b)). In addition, the THD of input current is observed

TABLE 2 Comparison of proposed charger configuration with various existing charger configurations

Topology	[20]	[25]	[26]	[27]	[30]	[28]	[29]	[23]	[24]	[21]	Proposed
total components	13	15	22	23		11		14	10	9	9
power switches	4	2	2	6	1	3	4	2	2	2	3
power diodes	4	3	8	10	5	2	6	2	2	2	2
inductors	0	5	6	3	3	2	4	3	3	1	2
auxiliary capacitors	0	3	4	1	2	0	2	2	1	2	1
device's voltage stress	high	high	high	high	high	high	high	high	high	high	low
device's current stress	Less	more	less	less	more	less	more	more	more	less	high
ripple in input current	less	less	less	less	more	less	less	more	less	high	low
ripple in output voltage	less	less	less	less	more	less	less	less	less	less	low
devices in conduction	4	1	2	6	3	3	5	1	3	2	3
operation mode	ccm	ccm	ccm	ccm	dcm	ccm	dcm	ccm	dcm	dcm	dcm
sensors	3	2	2	3	2	4	2	2	1	2	1
maximum efficiency (%)	98	91	88	93	N/R	95	96.9	N/R	95	94.3	95
power rating (W)	3.5k	5k	500	1.5k	850	1k	1.65k	N/R	200	100	2k

TABLE 3 Parameters used in the experimental study

System Parameters	Value
Input inductor (L_g)	2 mH
Auxiliary capacitor (C_A)	50 µF
Output inductor (L_0)	30 µH
Output capacitor (C_0)	500 µF
Switching frequency (f_s)	20 kHz
AC grid	120V rms
Battery pack	400V, 5Ahr
DSP controller	TMS320F28335
System power rating	2kW
Power switches	NTE3300
Power diodes	STTH1004FP

FIGURE 7 Experimental results of proposed charger for rated power of 2kW.

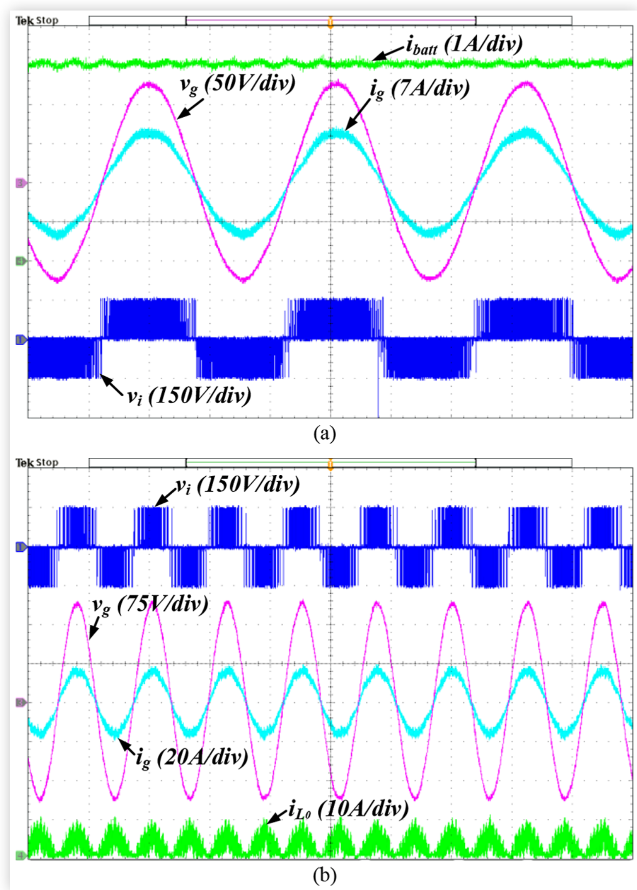

to be around 2.8% at power rating of 2kW. The THD in grid current at various power levels have been given in Table 4. It can also be observed from Fig. 7(a) that the battery current is regulated at an average current of 5A. Fig. 7(b) shows the current through output inductor (i_{L0}) and it is evident that the output inductor is operating in DCM. Even though the output inductor is having the high ripple in current, a higher efficiency (≈95%) of the converter is achieved due to lower stress across power devices and lesser devices in conducting in the any mode of operation. The efficiencies corresponding to the various outpower levels of the proposed charger are given in Fig. 8. It can be seen from the Fig. 8 that the proposed converter exhibits highest efficiency (≈95%) at 1.5kW and 94.1% at rated power of 2kW. The full loss distribution of all semiconductor devices in the proposed charger for 2kW rated power is given in Table 5. It can be observed from Table 5 that most of the losses in the converter are contributed by power switches ($S_{1\sim3}$). The losses in the power devices are estimated by using the expressions in [31] with the details mentioned in the datasheet of power devices. From the experimental studies, it can be understood that the theoretically estimated efficiency and experimental efficiencies are well matching.

To check the dynamic performance of the proposed charger configuration, the transient studies are performed, and the corresponding experimental results are shown in Fig. 9. First, the battery current reference to the current controller is changed from 2.5A to 5A (i.e., power reference is changed from 1kW to 2kW), it can be understood from Fig. 9(a) that the grid current (i_g) is changed from 8.3A RMS to 16.67A RMS.

TABLE 4 THD with respect to power output

Output power (W)	PF	THD (%)
200	0.989	4.37
400	0.99	4.25
600	0.99	4.1
800	0.991	3.8
1000	0.992	3.69
1200	0.992	3.42
1400	0.993	3.3
1600	0.993	2.93
1800	0.995	2.84
2000	0.996	2.8

FIGURE 8 Efficiency of proposed charger for various output power levels.

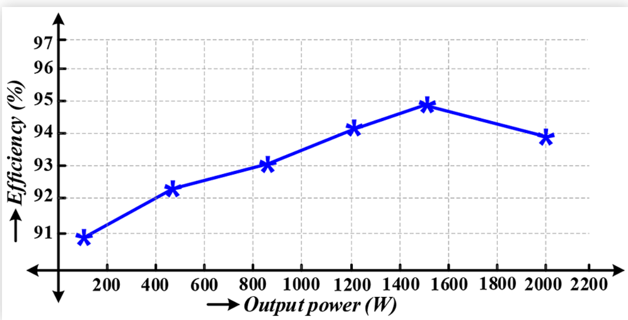

TABLE 5 Loss distribution between various power components

Power component	Loss (W)
Switches	38
Diodes	14
Grid inductor	12
Auxiliary capacitor	2
Output inductor	22
Output capacitor	16
Other	25
Total	128
Efficiency	94.1%

From Fig. 9(a), it can also be observed that grid current is adjusted accurately without any high transient in the current. Similarly, in Fig. 9(b), the battery reference current is changed from 5A to 2.5A which corresponds to the power changes from 2kW to 1kW, the input grid current is perfectly adjusted without any undershoot with nearly unity power factor (UPF). From all the experimental studies (Fig. 7, Fig. 8, and Fig. 9), it can be clearly observed that input current (i_g) is properly adjusted as per the battery current reference while maintaining the input current in a perfect sinusoidal nature with accurate PFC and lesser THD. In addition, the efficiencies of various existing charger configurations are compared and shown in Fig. 10.

FIGURE 9 Experimental results correspond to the transient studies.

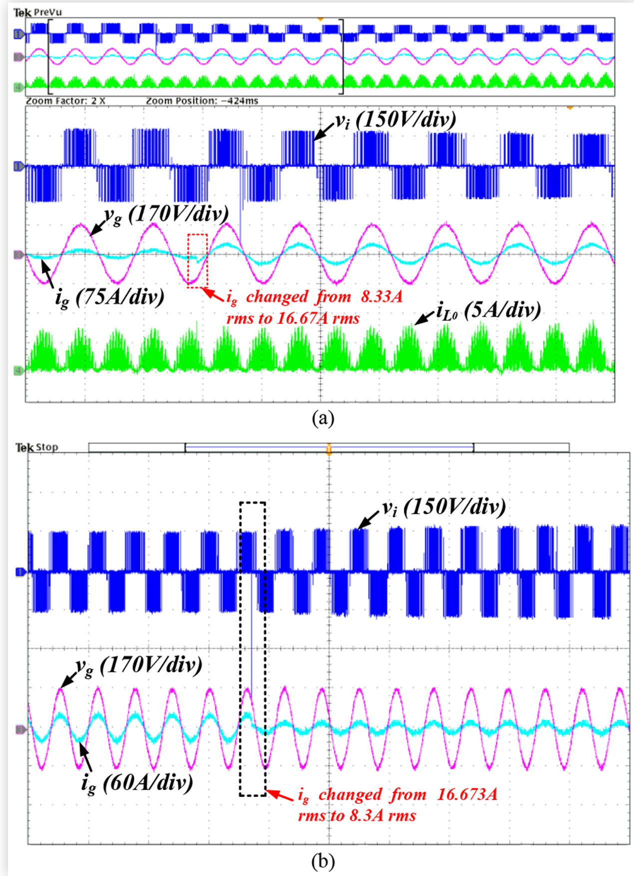

FIGURE 10 Efficiency comparison proposed charger with existing charger configurations.

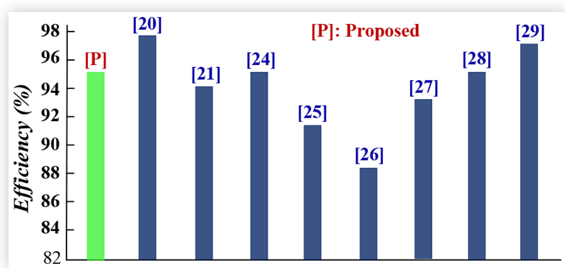

Summary/Conclusions

This paper proposed and investigated a novel Cuk based optimized component count PFC on-board EV charger which uses only one current sensor to charge the battery pack from the utility grid. The proposed EV charger's output inductor is operated in DCM to attain natural PFC at the AC grid and thus it reduces the requirement of sensors which minimizes the size and cost of the system. The reduction in size and cost of the system increases the power density and reliability of the total system. In addition, the proposed EV charger has lower voltage stress across the semiconductor devices compared to existing PFC EV charger configurations which helps in reducing the switching losses and thus improved the overall efficiency of the system. Further, only three power devices are in conduction in any mode of operation which enormously reduces the conduction losses and guarantees the proper thermal management of converter. The main benefits of this proposed work are simple EV charger configuration, accuracy of the closed loop control and feasibility for the practical application. In addition, this paper briefly discusses the existing EV charger configurations and their drawbacks. The experimental results validate the design of the proposed configuration. It can be observed from the experimental results that the THD of grid current is 2.8% with power factor of 0.996 at power rating of 2kW.

References

1. Gumrukcu, E. et al., "Impact of Cyber-attacks on EV Charging Coordination: The Case of Single Point of Failure," in *2022 4th Global Power, Energy and Communication Conference (GPECOM)*, Nevsehir, Turkey, 2022, 506-511, doi:10.1109/GPECOM55404.2022.9815727.
2. Moghassemi, A., Padmanaban, S., Ramachandaramurthy, V.K., Mitolo, M. et al., "A Novel Solar Photovoltaic Fed TransZSI-DVR for Power Quality Improvement of Grid-Connected PV Systems," *IEEE Access* 9 (2021): 7263-7279.
3. Buraimoh, E., Aluko, A.O., Oni, O.E., and Davidson, I.E., "Decentralized Virtual Impedance- Conventional Droop Control for Power Sharing for Inverter-Based Distributed Energy Resources of a Microgrid," *Energies* 15, no. 12 (2022): 4439.
4. Timilsina, L., Badr, P.R., Hoang, P.H., Ozkan, G. et al., "Battery Degradation in Electric and Hybrid Electric Vehicles: A Survey Study," *IEEE Access* 11 (2023): 42431-42462.
5. Hoang, P., Ozkan, G., Badr, P., Timilsina, L. et al., "A Prognostic Based Control Framework for Hybrid Electric Vehicles," SAE Technical Paper 2022-01-0352 (2022).
6. Hoang, P.H., Ozkan, G., Badr, P.R., Timilsina, L. et al., "Integrating Degradation Forecasting Into Distribution Grids' Advanced Distribution Management Systems," *International Journal of Electrical Power & Energy Systems* 150 (2023): 109071.
7. Buraimoh, E. and Davidson, I.E., "Simplified LCL Filter State Space Modeling and Small Signal Stability Analysis of Inverter Based Microgrid," in *2021 IEEE PES/IAS Power Africa*, Nairobi, Kenya, 2021, 1-5.
8. Buraimoh, E. and Davidson, I.E., "Fault Ride-Through Analysis of Current- and Voltage-Source Models of Grid Supporting Inverter-Based Microgrid," *IEEE Canadian Journal of Electrical and Computer Engineering* 44, no. 2 (2021): 189-198.
9. Metwly, M.Y., Abdel-Majeed, M.S., Abdel-Khalik, A.S., Hamdy, R.A. et al., "A Review of Integrated On-Board EV Battery Chargers: Advanced Topologies, Recent Developments and Optimal Selection of FSCW Slot/Pole Combination," *IEEE Access* 8 (2020): 85216-85242.
10. Metwly, M.Y., Maximos, F.A., Ahmed, A.T., Hawam, A.S. et al., "Design Case Study of a Nine-Phase Integrated On-Board Battery Charger," in *Proceeding 20th International Middle East Power System Conference (MEPCON)*, December 2018, 815-821.
11. Shi, C., Tang, Y., and Khaligh, A., "A Single-Phase Integrated Onboard Battery Charger Using Propulsion System for Plug-In Electric Vehicles," *IEEE Trans. Veh. Technol.* 66, no. 12 (2017): 10899-10910.
12. Kwon M. and Choi S., "An Electrolytic Capacitorless Bidirectional EV Charger for V2G and V2H Applications," *IEEE Trans. Power Electron.*, vol. 32, no. 9, pp. 6792-6799, Sep. 2017.
13. Zarkab, M., Singh, B., and Panighiri, B.K., "Performance Enhancement of Single-Phase Two-stage AC-DC Converter with Reduced DC-link Capacitance," *IEEE Transactions on Industry Applications*, doi:10.1109/TIA.2023.3286381.
14. Meng, L., Shu, Z., Lei, Y., Yan, H. et al., "Optimal Input and Output Power Quality Control of Single-Phase Ac–Dc–Dc Converter with Significant Dc-Link Voltage Ripple," *IEEE Trans. on Indus. Electron.* 67, no. 12 (2020): 10366-10376.
15. Xue, L., Shen, Z., Boroyevich, D., Mattavelli, P. et al., "Dual Active Bridge-Based Battery Charger for Plug-In Hybrid Electric Vehicle with Charging Current Containing Low Frequency Ripple," *IEEE Trans. On Power Electron.* 30, no. 12 (2015): 7299-7307.
16. Parvez Akter, M., Mekhilef, S., Mei Lin Tan, N., and Akagi, H., "Modified Model Predictive Control of a Bidirectional Ac–Dc Converter Based on Lyapunov Function for Energy Storage Systems," *IEEE Trans. on Indus. Electron.* 63, no. 2 (2016): 704-715.
17. Meher, S.R. and Singh, R.K., "A Standard Two Stage On-Board Charger with Single Controlled PWM and Minimum Switch Count," *IEEE Transactions on Industry Applications*, doi:10.1109/TIA.2023.3267334.
18. Gujar, H.R. and Panchade, V.M., "A Two-Stage Fast-Charging Technique for Electric Vehicle Charging," in *2022 International Conference on Smart Generation Computing, Communication and Networking (SMART GENCON)*, Bangalore, India, 2022, 1-6.
19. Sameh Abdelmomen, M., Abdelsalam, I., and Hamad, M.S., "Two-Stage Single-Phase EV On-Board Charger Based on Interleaved Bridgeless AC-DC Converter," in *2023 5th International Youth Conference on Radio Electronics, Electrical and Power Engineering (REEPE)*, Moscow, Russian Federation, 2023, 1-6.
20. Musavi, F., Eberle, W., and Dunford, W.G., "A High-Performance Single-Phase Bridgeless Interleaved PFC Converter for Plug-in Hybrid Electric Vehicle Battery Chargers," *IEEE Transactions on Industry Applications* 47, no. 4 (2011): 1833-1843.
21. Fardoun, A.A., Ismail, E.H., Al-Saffar, M.A., and Sabzali, A.J., "New "Real" Bridgeless High Efficiency AC-DC Converter," in *2012 Twenty-Seventh Annual IEEE Applied Power Electronics Conference and Exposition (APEC)*, Orlando, FL, 2012, 317-323.

22. Fardoun, A.A., Ismail, E.H., Sabzali, A.J., and Al-Saffar, M.A., “New Efficient Bridgeless Cuk Rectifiers for PFC Applications,” *IEEE Trans. Power Electron.* 27, no. 7 (2012): 3292-3301.
23. Sahid, M.R., Yatim, A.H.M., and Muhammad, N.D., “A Bridgeless Cuk PFC Converter,” in *2011 IEEE Applied Power Electronics Colloquium (IAPEC)*, Johor Bahru, Malaysia, 2011, 81-85.
24. Mahdavi, M. and Farzaneh-Fard, H., “Bridgeless Cuk Power Factor Correction Rectifier with Reduced Conduction Losses,” *IET Power Electron.* 5, no. 9 (2012): 1733-1740.
25. Shukla, T. and Kalla, U.K., “A Single-Stage positive Cuk Converter based Charging System for Light Electric Vehicle Applications,” in *2021 IEEE 2nd International Conference on Smart Technologies for Power, Energy and Control (STPEC)*, Bilaspur, Chhattisgarh, India, 2021, 1-6.
26. Luckose, V., Kannan, R., Hasan, K.N.M., and Ibrahim, T.B., “A Two-Stage Interleaved Bridgeless SEPIC Based PFC Converter for Electric Vehicle Charging Application,” in *2022 IEEE Ninth International Conference on Communications and Electronics (ICCE)*, Nha Trang, Vietnam, 2022, 488-493.
27. Chaithanya, S. and Sindhu, M.R., “A PFC Based Onboard Battery Charger Using Isolated Full-Bridge DC-DC Converter for Electric Vehicle Application,” in *2022 IEEE IAS Global Conference on Emerging Technologies (GlobConET)*, 581-586, 2022.
28. Jeong, Y., Park, M., and Moon, G., “High-Efficiency Zero Voltage-Switching Totem-Pole Bridgeless Rectifier with Integrated Inrush Current Limiter Circuit,” *IEEE Trans. Ind. Electron.* 67, no. 9 (2020): 7421-7429.
29. Seok, H., Junyent-Ferré, A., Kwon, B.-H., and Kim, M., “Bridgeless Push–Pull Resonant AC/DC Converter Featuring Balanced Switching Loss Distribution,” *IEEE Transactions on Industrial Electronics* 69, no. 2 (2022): 1443-1453.
30. Bhati, N. and Kalla, U.K., “A Single Phase – Single Stage Improved Power Quality EV Charger for Small and Medium Power Application,” in *2021 IEEE 2nd International Conference on Smart Technologies for Power, Energy and Control (STPEC)*, 1-5, 2021.
31. Li, P., Wang, Q., and Lu, S., “Power Conversion Efficiency Calculation Models for Electric Vehicle Fast Charger System,” in *2018 13th IEEE Conference on Industrial Electronics and Applications (ICIEA)*, Wuhan, China, 2018, 316-321.

Definitions/Abbreviations

EV - Electric Vehicle
PF - Power Factor
PFC - Power Factor Correction
DCM - Discontinuous Conduction Mode
PFCC - Power Factor Correction Converter
PWM - Pulse Width Modulation
THD - Total Harmonic Distortion
Fig. - Figure
UPF - Unity Power Factor
RMS - Root Mean Square

ISSN 0148-7191